



Optical, electrical and chemical properties of PEO:I₂ complex composite films

Ahmad Telfah¹ · Qais M. Al-Bataineh^{1,2} · Elen Tolstik¹ · Ahmad A. Ahmad² · Ahmad M. Alsaad² · Riad Ababneh³ · Carlos J. Tavares⁴ · Roland Hergenröder¹

Received: 28 March 2022 / Revised: 29 August 2022 / Accepted: 28 September 2022
© The Author(s) 2022

Abstract

Synthesized PEO:I₂ complex composite films with different I₂ concentrations were deposited onto fused silica substrates using a dip-coating method. Incorporation of PEO films with I₂ increases the electrical conductivity of the composite, reaching a maximum of 46 mS/cm for 7 wt% I₂. The optical and optoelectronic properties of the complex composite films were studied using the transmittance and reflectance spectra in the UV-Vis region. The transmittance of PEO decreases with increasing I₂ content. From this study, the optical bandgap energy decreases from 4.42 to 3.28 eV as I₂ content increases from 0 to 7 wt%. In addition, the refractive index for PEO films are in the range of 1.66 and 2.00. ¹H NMR spectra of pure PEO film shows two major peaks at 3.224 ppm and 1.038 ppm, with different widths assigned to the mobile polymer chains in the amorphous phase, whereas the broad component is assigned to the more rigid molecules in the crystalline phase, respectively. By adding I₂ to the PEO, both peaks (amorphous and crystal) are shifted to lower NMR frequencies indicating that I₂ is acting as a Lewis acid, and PEO is acting as Lewis base. Hence, molecular iodine reacts favorably with PEO molecules through a charge transfer mechanism, and the formation of triiodide (I₃⁻), the iodite (IO₂⁻) anion, I₂ · · · PEO and I₂⁺ · · · PEO complexes. PEO:I₂ complex composite films are expected to be suitable for optical, electrical, and optoelectronic applications.

Keywords Polyethylene oxide (PEO) · Iodine (I₂) · Electrical conductivity · Absorption bands · Vibrational bands · Optical and optoelectronic properties · Thermal properties

✉ Ahmad Telfah
telfah.ahmad@isas.de

Extended author information available on the last page of the article

Introduction

Polyethylene oxide (PEO) is a crucial polymer electrolyte due to its low cost, high chemical and electrochemical stability, high stability in reduction processes, and good solubility of metal ions [1–6]. The importance of the PEO is for practical applications such as fuel cells, lithium-ion batteries, hybrid power supercapacitors [3, 7]. Incorporating inorganic ions into the polymer reduces transparency due to the absorption and scattering of electromagnetic photons from ionic agglomerates [8–11]. These complex composite films have tantalizing applications in advanced optoelectronic devices [12, 13].

The main reasons for choosing PEO as the host polymer in this study are the semi-crystalline nature [14], besides the low absorption of visible light [15, 16]. The electrical conductivity of the polymer increased by incorporation with electron donors or acceptors [17]. Iodine (I_2) was chosen as the electron acceptor dopant in the polymers because of its significant influence on the optical, electrical and dielectric properties [18, 19]. According to our previous study [20], PEO: I_2 is an effective complex composite because of the significant variations in ionic conductivity and dielectric properties.

Previous work [20] investigated the effect of iodine doping in PEO films on dielectric relaxation, X-ray photoelectron spectroscopy, and morphological properties. To further tune the optical, optoelectronic and electrical properties, such as refractive index, optical bandgap, and electrical conductivity, and to better understand the nature of the interactions in PEO, this study presents a composite of PEO polymer with different doping levels with inorganic filler I_2 . The effect of varying ionic concentrations of PEO: I_2 complex composite films on optical and electrical properties is discussed. Furthermore, this study aims to understand the doping mechanism of PEO: I_2 complex composite.

Experimental sections

Sample preparation

Polyethylene oxide (PEO) of M_w 300.000 g/mol and Iodine (I_2) of M_w 253.8089 g/mol were obtained from Sigma-Aldrich; all solutions were prepared in absolute methanol (MeOH). A polymeric stock solution of PEO/MeOH was prepared by dissolving 1.0 g PEO in 100 mL MeOH by stirring for 5 h at 45 °C. The ionic stock solution of I_2 /MeOH was prepared by dissolving 0.1 g of I_2 in 100 mL MeOH by stirring for 5 h at room temperature. The complex composite solutions with 0, 1, 3, 5, and 7 wt% of I_2 were prepared by mixing 20 mL of PEO/MeOH with a calculated volume of I_2 /MeOH by ultrasonic water bath until the solution became a yellow homogeneous solution. PEO: I_2 complex composite films were deposited on fused silica substrates by the dip-coating technique for 2 h. After that, PEO: I_2 complex composite films were accomplished by drying the

resulting films at room temperature for 24 h. A mathematical model proposed by Al Bataineh et al. was used to calculate the film thickness, which turned out to be around 500 nm [21].

Characterization

The doping mechanism for the PEO:I₂ complex composite was investigated by analyzing the chemical structure using an FTIR Microscope HYPERION 3000 from Bruker and HN MAS NMR (600.13 MHz, Bruker AVIII-600 spectrometer). In addition, the electrical conductivity and pH measurements were also performed with SevenGo Duo SG23 conductivity-pH, and the absorption bands for the composite solution were examined with a UV-Vis spectrophotometer (Hitachi U-3900H) with a total internal integrating sphere. Thermal stability was investigated by thermogravimetric analysis (NETZSCH Premier Technologies, Exton, PA, USA).

Results and discussion

FTIR and NMR spectroscopies

Figure 1 shows the chemical structure of pure PEO and PEO:I₂ composites. The FTIR spectra show the typical vibrational bands of PEO, the vibrational band

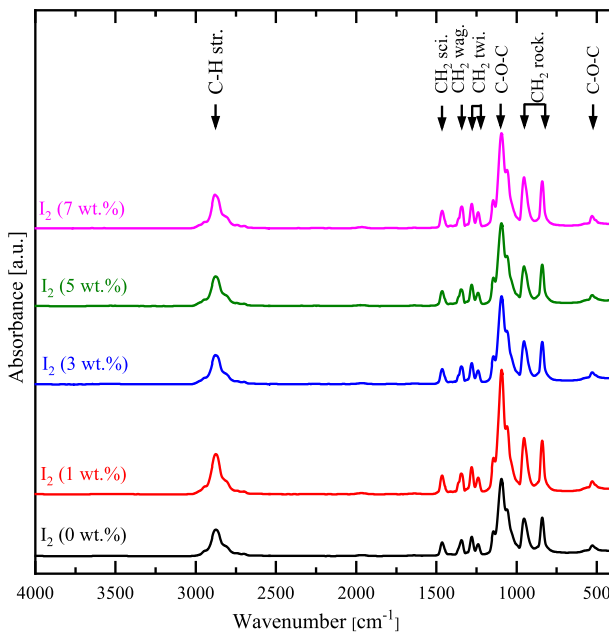


Fig. 1 FTIR spectra of pure PEO and PEO:I₂ complex composites with varying I₂ doping concentrations

observed at 2880 cm^{-1} represents the stretching C–H bonds, 1466 cm^{-1} represents the scissoring CH_2 bonds, 1340 cm^{-1} represents the wagging CH_2 bonds, 1276 and 1235 cm^{-1} represent the twisting CH_2 bonds, 955 and 840 cm^{-1} represent the rocking CH_2 bonds, and 527 cm^{-1} represents the bending C–H bonds. Moreover, the triplet peak of the C–O–C stretching band at a maximum of 1088 cm^{-1} confirms the semicrystalline phase of PEO [22]. It is clear that the introduction of I_2 into PEO has shifted the peak from 531 into 529 cm^{-1} , indicating the appearance of C–I stretching vibrations and thus incorporating iodine with the polymer matrix. In addition, it can be seen that apparent changes in linewidth and peak position are observed with increasing I_2 concentration. These changes represent the difference in the electronegativity between iodine and the polymer atoms, which can significantly affect the neighbouring group frequencies [18]. Furthermore, the change in intensity, linewidth and band position of the triplet peak of the C–O–C stretching band confirms the change in the degree of crystallinity [22].

^1H NMR spectra of pure PEO film show two major peaks at 1.038 ppm and 3.224 ppm , with different widths (Fig. 2). Characteristically, the narrow component can be assigned, without ambiguity, to the mobile polymer chains in the amorphous phase, whereas the broad component is assigned to the more rigid molecules in the crystalline phase. Therefore, the peaks at 1.132 ppm and 3.174 ppm belong to the crystalline and the amorphous phase, respectively [23]. The amorphous phase peak has a symmetric shape at room temperature, while the NMR peak of the crystalline phase is still a broad asymmetric convoluted peak indicating that the crystalline phase is still in the rigid glassy form. Introducing I_2 into the PEO matrix leads to increasing the linewidths of both peaks, but the changes are more pronounced in the peak associated with the amorphous phase. By adding I_2 to the PEO, both peaks (amorphous and crystal) were shifted to the lower NMR frequencies indicating that the protons

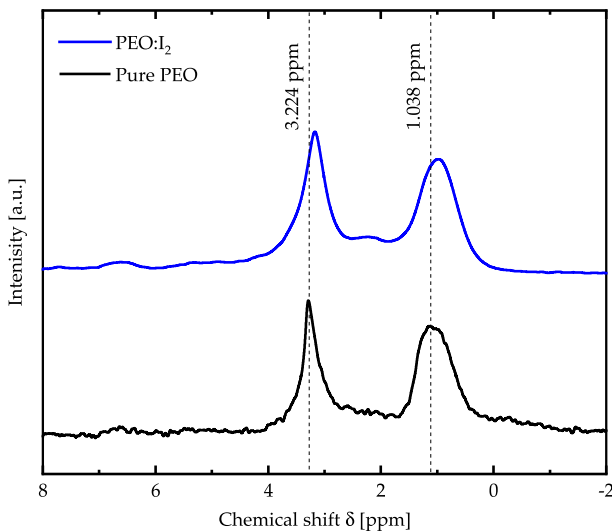


Fig. 2: ^1H NMR spectra of pure PEO and PEO: I_2 complex composite

in PEO have a higher electron density. This means that I_2 is acting as a Lewis acid, and PEO is acting as Lewis bases, hence, molecular iodine reacts favorably with PEO molecules through a charge transfer mechanism, to form charge transfer complexes (CTCs) as confirmed by electron spin resonance spectroscopy [24]. Additionally, the complexation also confirmed by the high-resolution XPS of the lower binding component confirmed the formation of triiodide (I_3^-) [25], the iodite (IO_2^-) anion, $I_2 \cdots PEO$ and $I_2^+ \cdots PEO$ complexes [26–28]. Additionally, XPS confirmed that $I_2 \cdots PEO$ complex is shifted to a higher binding energy relative to the molecular I_2 , due to the partial positive charge on the I_2 caused by the interaction with the more electronegative oxygen atoms in PEO [17].

pH measurement and electrical conductivity

Figure 3a shows the pH measurement results of the PEO: I_2 complex composite solutions. pH values decrease as the I_2 concentration increases in the composite, which translates into increased solution acidity with doping. Figure 3b shows the electrical conductivity for PEO: I_2 complex composite solutions as a function of I_2 concentration. The electrical conductivity of the PEO: I_2 solution increased by four orders of magnitude with I_2 doping, with a maximum of 46 mS/cm being achieved with 7 wt% of I_2 . Additionally, the conductivity of the PEO: I_2 films also improves with increasing I_2 concentration (Fig. 3c). The low electrical conductivity value associated with pure PEO can be attributed to the van der Waals interactions in polymer and the charge carriers hopping in the amorphous phase in this polymer [29]. Introducing I_2 in the PEO matrix changes the gap-state occupation and, consequently, changes the electrical conductivity. Moreover, the electrical activity of iodine in the doped states can be affected by two factors: the first is related to the dangling bonds D^0 and H-atoms of PEO, and the second is due to the creation of other dangling bond states D^+ [30]. Also, iodine creates deep localized states in PEO, which leads to gap-state density changes by shifting the Fermi level and, consequently, increasing the electrical conductivity [31]. However, the electrical conductivity of the complex composite

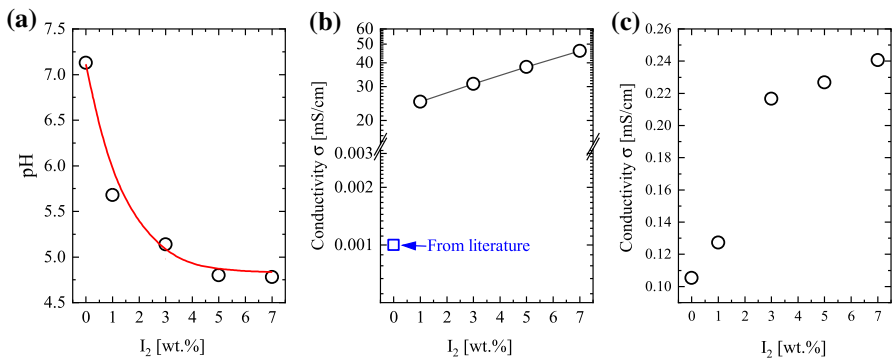


Fig. 3 a pH and b electrical conductivity of PEO: I_2 composite solutions versus I_2 [wt.%], and c Electrical conductivity of PEO: I_2 composite films versus I_2 [wt.%]

solutions is much higher than the electrical conductivity of the films, which can be attributed to the existence of diffusion of the iodine and the other factors that affect the electrical conductivity.

UV–Vis absorption spectroscopy

UV–Vis absorption spectroscopy was used to study the absorption bands of PEO: I_2 complex composites (Fig. 4). Incorporation of PEO with I_2 leads to a decrease in bandgap energy, shifting into the red region of the absorption bands and creating a new sub-band at 415.86 nm for 1 wt% I_2 concentration, being the latter band red-shifted to 441.04 nm for 7 wt% I_2 concentration. The absorbance spectra for PEO exhibit three transition bands with maxima at 216.69, 271.09, and 346.60 nm, with linewidths of 37.20, 70.66, and 191.62 nm, respectively. These three transitions can be assigned to polyenic domains in PEO [32]. According to molecular orbital theory [33], there are three possible electronic transitions for PEO: at 5.722 eV attributed to $\pi \rightarrow \pi^*$ from unsaturated bonds [21], at 4.574 eV attributed to $n \rightarrow \pi^*$ from carbonyl C–O bonds [34], and at 3.578 eV attributed to $n \rightarrow \sigma^*$ from C–H bond.

The absorbance spectra of I_2 in PEO illustrate four bands around 220, 290, 360, and 440 nm, which are assigned to the absorption of complex formation between PEO and I_2 , I^- , I_3^- , and I_2 molecules, respectively [35, 36]. The absorption band between 440 and 500 nm represents the dissolving of I_2 in PEO, identical to the spectra of I_2 in alcohol and ethers [37]. The absorption shoulder typically appears at

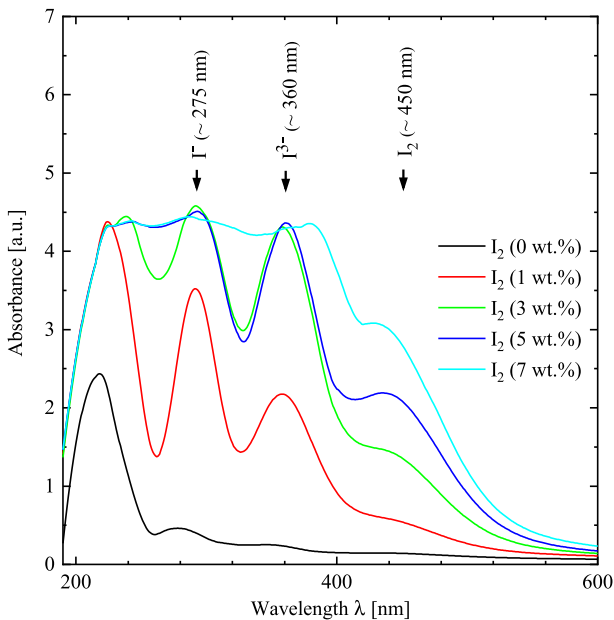


Fig. 4 Absorbance spectra for PEO: I_2 composite solutions

around 450 nm in thick PEO:I₂ composite films, confirming that the iodine–iodide equilibrium is still present in PEO [38]. In conclusion, the dissolution of I₂ in the PEO can be described as [39, 40]:



Thermogravimetric analysis

Thermogravimetric analysis (TGA) was used to study the thermal stability of PEO:I₂ complex composites at temperatures up to 400 °C (Fig. 5a). The weight loss (%) of PEO:I₂ complex composites decreases slightly in the range of 40–200 °C, due to water adsorption, intermolecular/intramolecular bonding, and chemical stability. Figure 5b shows the FTIR spectra for pure PEO and PEO:I₂ (5 wt%) at different annealing temperatures. It is clear that at 200 °C there are no bond breaks. Between 200 and 300 °C, the weight loss (%) of pure PEO and PEO:I₂ complex composites decreases again, which reflects the elimination of C–O stretch, C–H bend, and –CH₂ stretch for pure PEO, and C–O stretch, C–H bend and –CH₂ stretch in addition to C–I stretch for PEO:I₂ composites, as shown in Fig. 5b. The weight loss (%) of pure PEO and PEO:I₂ complex composites decreases sharply above 300 °C, attributed to the breaking of all bonds in the composites, as shown in Fig. 5b.

The maximum weight loss rate determined by DTG was observed at 325 °C for PEO, with this maximum rate shifting to higher temperatures as the I₂ content increases in PEO. This indicates that the PEO:I₂ complex composite has higher

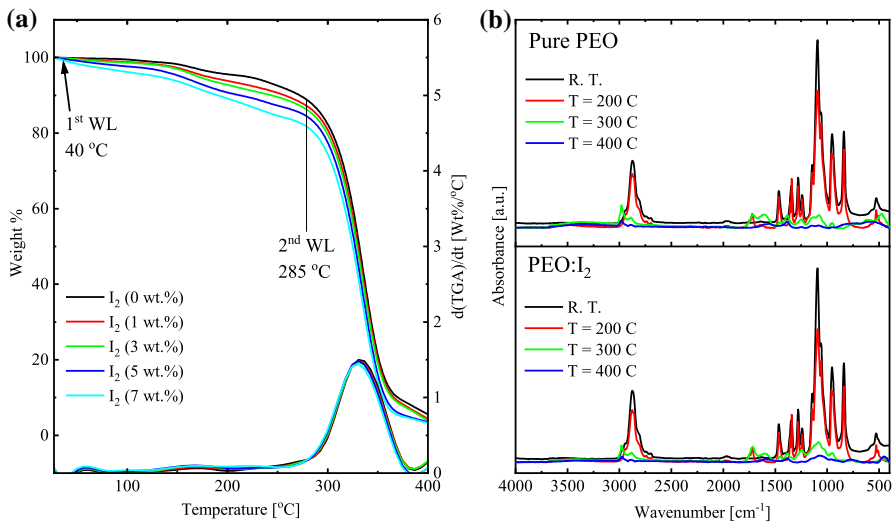


Fig. 5 **a** TGA and d(TGA) curves for PEO:I₂ composite films for varying I₂ concentration, **b** FTIR spectra of pure PEO and PEO:I₂ (5 wt%) films for varying annealing temperatures

thermal stability compared to pure PEO. The increase in thermal stability of the PEO:I₂ complex composite can be attributed to the difference in ionic radii in which I⁻—ionic radii (1.33 Å) is lower than O²⁻—ionic radii (1.40 Å) [41]. Therefore, PEO:I₂ complex composite films are expected to be stable at temperatures below 385 °C, where most optical, optoelectronic, and electrical applications can be achieved.

Optical and optoelectronic properties

The transmittance spectrum for PEO film increases to 93% as the wavelength increases from 250 to 400 nm and then reaches a plateau in the range of 400–700 nm (Fig. 6a). PEO:I₂ complex composite films have lower transmittance than pure PEO film, albeit still having a high transmittance in the visible region, such as for PEO:I₂ films with 7 wt% I₂ with an average of 86%. The influence of I₂ content with respect to PEO on the transmittance is the nonlinear effect. Broad dips in the transmittance spectra of the PEO:I₂ films in the range of 350–450 nm are attributed to the X to B band transfer of I₂. The absorption edge is continuously shifted into the red region with increasing I₂ concentration, indicating a continuous reduction in bandgap energy due to the excitation of valence band electrons to the conduction band of I₂ ions. The reflectance spectra (Fig. 6b) show the opposite curve progression with the transmittance spectra. The reflectance of PEO film decreases from 12.0 to 6.2% as the wavelength increases from 350 to 700 nm. Adding I₂ to the PEO film increases reflectance values in the visible region.

The extinction coefficient (*k*) is related to the absorption coefficient according to the equation $k = \alpha \lambda / 4\pi$ [42]. Figure 6c shows the *k*-spectra for PEO:I₂ complex composite

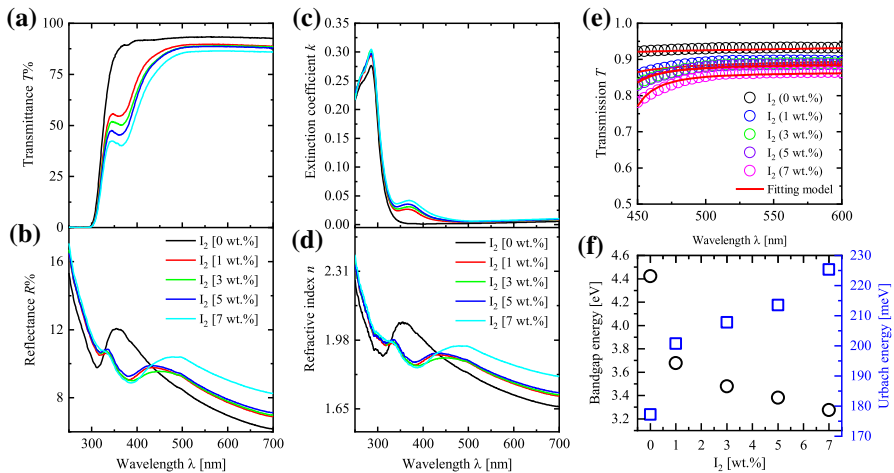


Fig. 6 **a** Transmittance, **b** reflectance, **c** extinction coefficient, and **d** refractive index spectra of PEO:I₂ films for different I₂ concentrations, **e** Transmittance spectra of PEO: I₂ films for different I₂ concentrations; experimental (colored circles) and model calculated (solid red lines). **f** Band-gap energy (*E_g*) and Urbach energy of PEO:I₂ films as a function of I₂ concentrations (colour figure online)

films. k -values decrease significantly below the absorption edge into the visible range, indicating that photons pass through the film in this range. As I_2 content increases in the PEO films, the light energy loss also increases due to scattering and absorption [43]. The refractive index, n , for the PEO: I_2 complex composite films was deduced from the following equation $n = (1 + R/1 - R) + \sqrt{(4R/(1 - R)^2) - k^2}$ (Fig. 6d) [42]. The n -values for a pure PEO film decrease from 2.00 to 1.66 as the incident photon wavelength increases from 250 to 700 nm. Furthermore, increasing the I_2 concentration in PEO films results in a concomitant increase in the refractive index, attributed to the iodine ions condensation into polyiodide clusters in the PEO films [44]. The wide drop in the refractive index spectra in the range of 250–350 nm for pure PEO film and 300–450 nm for PEO: I_2 films can be attributed to the resonance effect between the incident photons and the electrons in the films [45].

A mathematical model developed by Al Bataineh et al. was used to investigate the bandgap energy (E_g) for PEO: I_2 complex composite films according to the following relationship [21]:

$$T(\lambda) = e^{-\frac{4\pi d}{\lambda} \frac{A(hc/\lambda - E_g)^2}{(hc/\lambda)^2 - B(hc/\lambda) + C}} \tag{3}$$

where $hc = 1239.84$ eV nm, and A, B, C are fitting constants. Figure 6e shows the model fit of transmission values for pure PEO and PEO: I_2 complex composite films. Figure 6f shows the bandgap energy variation obtained from this model. The bandgap energy of pure PEO film is 4.42 eV. As I_2 content increased in the PEO: I_2 films the band-gap decreases to a minimum of 3.28 eV for 7 wt% of I_2 . The interaction between PEO and I_2 is an oxidative interaction, which means that the radical cation in the PEO is formed with iodine anion and consequently forms polarons and decreases the bandgap energy [20].

Urbach energy, E_U , describes the disorder degree in the films by an empirical rule based on the following equation $\alpha = \alpha_0 \exp(h\nu/E_U)$ [46]. The E_U values can be determined by plotting $\ln(\alpha)$ as a function of $h\nu$. Figure 6f shows the Urbach energy variation for all PEO: I_2 films as a function of I_2 concentration. The Urbach energy for pure PEO film is 177.2 meV. This parameter increases with I_2 content up to a maximum of 225.3 meV for 7 wt% of I_2 . This trend indicates an increase in the disorder of the films in addition to the increase in organic–inorganic interaction [47].

To understand the influence of I_2 doping on the optical and optoelectronic properties of the complex composite films, models developed by Wemple–DiDomenico (WDD) [48, 49], Sellmeier [50], and Spitzer-Fan [51] were applied using the following equations, respectively,

$$(n^2 - 1)^{-1} = \frac{E_0}{E_d} - \frac{h\nu^2}{E_0 E_d} \tag{4}$$

$$n^2 - 1 = \frac{S_0 \lambda_0^2}{1 - (\lambda_0^2/\lambda^2)} \tag{5}$$

$$n^2 = \epsilon' = \epsilon_\infty - \frac{1}{4\pi^2\epsilon_0} \left(\frac{e^2}{c^2} \right) \left(\frac{N_c}{m^*} \right) \lambda^2 \quad (6)$$

Table 1 shows essential optical and optoelectronic parameters for pure PEO and PEO:I₂ complex composite films for different I₂ concentrations. Effective single oscillator energy (E_0) and dispersive energy (E_d) (Eq. 1) is used for the design of dispersive and optical communication devices. Increasing I₂ in PEO:I₂ films leads to a decrease in E_0 and conversely an increase in E_d , resulting from decreasing binding energy between the film elements [52]. Average oscillator wavelength (λ_0) values increase from 197.13 to 198.53 nm, and oscillator length strength (S_0) values increase from 3.975×10^{-5} to 4.359×10^{-5} as I₂ content increases in PEO to 7 wt%. Consequently, the increase in λ_0 and S_0 is due to the decline in surface morphology of films with introducing I₂ in PEO films. The high-frequency dielectric constant (ϵ_∞) for PEO film is 3.410. This value increases to 3.949 for 7 wt% of I₂ in PEO. This also increases the charge carriers concentration from 6.688×10^{26} to 7.029×10^{26} atoms/m³ with the same increase in doping.

Conclusions

The doping mechanism for PEO:I₂ was studied using FTIR spectroscopy, pH, electrical conductivity, UV–Vis absorbance spectroscopy, and TGA. The changes in peak position and linewidth of the absorption spectra are due to the incorporation of PEO and I₂. In addition, introducing I₂ into PEO leads to a shift of the peak at 535 cm⁻¹, due to increased C–I stretching vibrations. Electrical conductivity increases concomitantly with increasing I₂ doping in PEO films, while pH values decrease due to increasing solution acidity.

TGA with FTIR analysis at different annealing temperatures showed that the weight loss of pure PEO and PEO:I₂ complex composites decreases slightly from 40 to 200 °C, attributed to the adsorbed water, intermolecular/intramolecular bonding and chemical stability. In addition, between 200 and 300 °C, the weight loss of pure PEO and PEO:I₂ complex composites also decreases, due to the elimination of C–O stretch, C–H bend, and –CH₂ stretch for pure PEO, and C–O stretch, C–H bend and –CH₂ stretch in addition to C–I stretch. Above 300 °C, the weight loss of pure PEO and PEO:I₂ complex composites decreases sharply, attributed to bond breaking the film composites.

The transmittance of the PEO film decreases with increasing I₂ content, while the optical band gap energy decreases from 4.42 to 3.28 eV as I₂ content increases from 0 to 7 wt%. In addition, the refractive index for PEO film has values ranging between 1.66 and 2.00 as the wavelength decreases from 700 to 350, and the average values of the refractive index increase as the concentration of I₂ is increased up to 7 wt%.

The ¹H NMR peak appearing at 1.038 ppm can be assigned to the mobile polymer chains in the amorphous phase while the peak at 3.224 ppm is assigned to the more rigid molecules in the crystalline phase which was still in the rigid glassy form

Table 1 Optical and optoelectronic parameters of pure PEO and PEO:I₂ complex composite films for various I₂ concentrations

Parameter	PEO	PEO:I ₂ 1 wt%	PEO:I ₂ 3 wt%	PEO:I ₂ 5 wt%	PEO:I ₂ 7 wt%
Effective single oscillator, E_0 (eV)	6.282	6.279	6.249	6.243	6.250
Dispersion energy, E_d (eV)	9.706	10.547	10.391	10.401	10.738
Average oscillator wavelength, λ_0 (nm)	197.133	197.379	198.477	198.348	198.526
Oscillator length strength, $S_0 \times 10^{-5}$	3.975	4.312	4.221	4.234	4.359
Density of states, $N_c/m^* \times 10^{37}$ (m ⁻³ kg ⁻¹)	1.669	1.827	1.791	1.700	1.754
Charge carrier density, $N_c \times 10^{26}$ (m ⁻³)	6.688	7.323	7.180	6.830	7.029
High-frequency dielectric constant, ϵ_{∞}	3.410	3.644	3.650	3.652	3.949

at room temperature. By adding I_2 to the PEO, both peaks (amorphous and crystal) were shifted to the lower NMR frequencies indicating that I_2 is acting as a Lewis acid, and PEO is acting as Lewis bases and the formation of triiodide (I_3^-), the iodite (IO_2^-) anion, $I_2 \cdots PEO$ and $I_2^+ \cdots PEO$ complexes.

Acknowledgements The scientific support by the Ministerium für Innovation, Wissenschaft und Forschung des Landes Nordrhein-Westfalen, the Senatsverwaltung für Wirtschaft, Technologie und Forschung des Landes Berlin, and the Bundesministerium für Bildung und Forschung is gratefully acknowledged. This study was supported by the German Ministry of Research and Education (ERK-Casting, 16GW0262K), and the Drug Discovery Hub Dortmund (DDHD). The authors would like to acknowledge Jordan University of Science and Technology. Our thanks also to Prof. Mohammad-Ali H. Al-Akhras for helping our members to use the biomedical laboratory.

Funding Open Access funding enabled and organized by Projekt DEAL.

Open Access This article is licensed under a Creative Commons Attribution 4.0 International License, which permits use, sharing, adaptation, distribution and reproduction in any medium or format, as long as you give appropriate credit to the original author(s) and the source, provide a link to the Creative Commons licence, and indicate if changes were made. The images or other third party material in this article are included in the article's Creative Commons licence, unless indicated otherwise in a credit line to the material. If material is not included in the article's Creative Commons licence and your intended use is not permitted by statutory regulation or exceeds the permitted use, you will need to obtain permission directly from the copyright holder. To view a copy of this licence, visit <http://creativecommons.org/licenses/by/4.0/>.

References

1. Bresser D, Lyonnard S, Iojoiu C, Picard L, Passerini S (2019) Decoupling segmental relaxation and ionic conductivity for lithium-ion polymer electrolytes. *Mol Syst Des Eng* 4:779
2. Scrosati B, Vincent CA (2000) Polymer electrolytes: the key to lithium polymer batteries. *Mrs Bull* 25(3):28–30
3. Xue Z, He D, Xie X (2015) Poly(ethylene oxide)-based electrolytes for lithium-ion batteries. *J Mater Chem A* 3(38):19218–19253
4. Mindemark J, Lacey MJ, Bowden T, Brandell D (2018) Beyond PEO—alternative host materials for Li⁺-conducting solid polymer electrolytes. *Prog Polym Sci* 81:114–143
5. Lin D, Yuen PY, Liu Y, Liu W, Liu N, Dauskardt RH, Cui Y (2018) A silica-aerogel-reinforced composite polymer electrolyte with high ionic conductivity and high modulus. *Adv Mater* 30(32):1802661
6. Aldalur I, Martinez-Ibañez M, Piszcz M, Rodriguez-Martinez LM, Zhang H, Armand M (2018) Lowering the operational temperature of all-solid-state lithium polymer cell with highly conductive and interfacially robust solid polymer electrolytes. *J Power Sources* 383:144–149
7. Karmakar A, Ghosh A (2012) Dielectric permittivity and electric modulus of polyethylene oxide (PEO)–LiClO₄ composite electrolytes. *Curr Appl Phys* 12(2):539–543
8. Liu J-G, Ueda M (2009) High refractive index polymers: fundamental research and practical applications. *J Mater Chem* 19(47):8907–8919
9. Hassan M, Reddy KR, Haque E, Minett AI, Gomes VG (2013) High-yield aqueous phase exfoliation of graphene for facile nanocomposite synthesis via emulsion polymerization. *J Colloid Interface Sci* 410:43–51
10. Reddy KR, Sin BC, Ryu KS, Kim J-C, Chung H, Lee Y (2009) Conducting polymer functionalized multi-walled carbon nanotubes with noble metal nanoparticles: synthesis, morphological characteristics and electrical properties. *Synth Met* 159(7–8):595–603

11. Tao P, Li Y, Rungta A, Viswanath A, Gao J, Benicewicz BC, Siegel RW, Schadler LS (2011) TiO₂ nanocomposites with high refractive index and transparency. *J Mater Chem* 21(46):18623–18629
12. Mosley DW, Auld K, Conner D, Gregory J, Liu X-Q, Pedicini A, Thorsen D, Wills M, Khanarian G, Simon ES (2008) High performance encapsulants for ultra high-brightness LEDs. In: *Light-emitting diodes: research, manufacturing, and applications XII*, vol 6910. International Society for Optics and Photonics, p 691017
13. Nakamura T, Fujii H, Juni N, Tsutsumi N (2006) Enhanced coupling of light from organic electro-luminescent device using diffusive particle dispersed high refractive index resin substrate. *Opt Rev* 13(2):104–110
14. Migdadi A, Ahmad AA, Alsaad AM, Al-Bataineh QM, Telfah A (2022) Electrical and thermal characterizations of synthesized composite films based on polyethylene oxide (PEO) doped by aluminum chloride (AlCl₃). *Polym Bull*. <https://doi.org/10.1007/s00289-022-04329-5>
15. Alsaad A, Al-Bataineh QM, Qattan I, Ahmad AA, Ababneh A, Albataineh Z, Aljarrah IA, Telfah A (2020) Measurement and ab initio Investigation of structural, electronic, optical, and mechanical properties of sputtered aluminum nitride thin films. *Front Phys* 8:115
16. Ohring M (2001) *Materials science of thin films*. Elsevier
17. Telfah A, Al-Akhras M-A, Al-Izzy KA, Ahmad AA, Ababneh R, Ahmad MJA, Tavares CJ, Hergenröder R (2022) Dielectric relaxation, XPS and structural studies of polyethylene oxide/iodine complex composite films. *Polym Bull* 79(6):3759–3778
18. Bazaka K, Jacob MV (2017) Effects of iodine doping on optoelectronic and chemical properties of polyterpenol thin films. *Nanomaterials* 7(1):11
19. Telfah M, Ahmad A, Alsaad A, Al-Bataineh QM, Telfah A (2022) Doping mechanism and optical properties of as-prepared polyvinyl chloride (PVC) doped by iodine thin films. *Polym Bull*. <https://doi.org/10.1007/s00289-022-04082-9>
20. Telfah A, Al-Akhras M-A, Al-Izzy KA, Ahmad AA, Ababneh R, Ahmad MJA, Tavares CJ, Hergenröder R (2021) Dielectric relaxation, XPS and structural studies of polyethylene oxide/iodine complex composite films. *Polym Bull* 79:1–20
21. Al-Bataineh QM, Alsaad A, Ahmad A, Telfah A (2020) A novel optical model of the experimental transmission spectra of nanocomposite PVC-PS hybrid thin films doped with silica nanoparticles. *Heliyon* 6(6):e04177
22. Noor S, Ahmad A, Talib I, Rahman MY (2010) Morphology, chemical interaction, and conductivity of a PEO-ENR50 based on solid polymer electrolyte. *Ionics* 16(2):161–170
23. Johansson A, Tegenfeldt J (1992) NMR study of crystalline and amorphous poly(ethylene oxide). *Macromolecules* 25(18):4712–4715
24. Danyluk S, Schneider W (1962) The electron spin resonance of non-alternant aromatic hydrocarbon-iodine complexes. *Can J Chem* 40(9):1884–1885
25. Kumar GR, Savariraj AD, Karthick S, Selvam S, Balamuralitharan B, Kim H-J, Viswanathan KK, Vijaykumar M, Prabakar K (2016) Phase transition kinetics and surface binding states of methylammonium lead iodide perovskite. *Phys Chem Chem Phys* 18(10):7284–7292
26. Zhang J, Song T, Zhang Z, Ding K, Huang F, Sun B (2015) Layered ultrathin PbI₂ single crystals for high sensitivity flexible photodetectors. *J Mater Chem C* 3(17):4402–4406
27. Salaneck W, Thomas H, Bigelow R, Duke C, Plummer E, Heeger A, MacDiarmid A (1980) Photoelectron spectroscopy of iodine-doped polyacetylene. *J Chem Phys* 72(6):3674–3678
28. Sherwood P (1976) NIST X-ray photoelectron spectroscopy database. *J Chem Soc Faraday Trans II* 72:1806
29. Masoud EM, El-Bellihi A-A, Bayoumy W, Mousa M (2013) Organic-inorganic composite polymer electrolyte based on PEO-LiClO₄ and nano-Al₂O₃ filler for lithium polymer batteries: Dielectric and transport properties. *J Alloys Compd* 575:223–228
30. Tyczkowski J (2004) *Electrical and optical properties of plasma polymers*. Plasma Polymer Films. Imperial College Press, pp 143–216
31. Arkhipov V, Heremans P, Emelianova E, Adriaenssens G, Bäessler H (2004) Charge carrier mobility in doped disordered organic semiconductors. *J Non-Cryst Solids* 338:603–606
32. El-Ghamaz N, Ghaly H (2016) Effect of chemical and physical doping with iodine on the optical and dielectric properties of poly(vinyl chloride). *Chem Phys Lett* 648:66–74
33. Fleming I (2011) *Molecular orbitals and organic chemical reactions*. Wiley

34. Al-Bataineh QM, Telfah M, Ahmad AA, Alsaad AM, Qattan IA, Baaziz H, Charifi Z, Telfah A (2020) Synthesis, crystallography, microstructure, crystal defects, optical and optoelectronic properties of ZnO:CeO₂ mixed oxide thin films. *Photonics* 7(4):112
35. Zidan HM, Abdelrazek EM, Abdelghany AM, Tarabiah AE (2019) Characterization and some physical studies of PVA/PVP filled with MWCNTs. *J Mater Res Technol* 8(1):904–913
36. Ryu SH, Cho H-B, Kim S, Kwon Y-T, Lee J, Park K-R, Choa Y-H (2018) The effect of polymer particle size on three-dimensional percolation in core-shell networks of PMMA/MWCNTs nanocomposites: properties and mathematical percolation model. *Compos Sci Technol* 165:1–8
37. Kumar A, Kumar V, Kumar M, Awasthi K (2018) Synthesis and characterization of hybrid PANI/MWCNT nanocomposites for EMI applications. *Polym Compos* 39(11):3858–3868
38. Wu G, Jia Z, Zhou X, Nie G, Lv H (2020) Interlayer controllable of hierarchical MWCNTs@C@Fe₂O₃ cross-linked composite with wideband electromagnetic absorption performance. *Compos A Appl Sci Manuf* 128:105687
39. Kim K-I, Kim D-A, Patel KD, Shin US, Kim H-W, Lee J-H, Lee H-H (2019) Carbon nanotube incorporation in PMMA to prevent microbial adhesion. *Sci Rep* 9(1):1–11
40. Karlsen EM, Spanget-Larsen J (2009) FTIR investigation of the reaction between pyridine and iodine in a polyethylene host. Formation of *N*-iodopyridinium polyiodide. *Chem Phys Lett* 473(4–6):227–232
41. Shariati A, Omidkhan M, Pedram MZ (2012) New permeation models for nanocomposite polymeric membranes filled with nonporous particles. *Chem Eng Res Des* 90(4):563–575
42. Ahmad A, Alsaad A, Al-Bataineh Q, Al-Naafa M (2018) Optical and structural investigations of dip-synthesized boron-doped ZnO-seeded platforms for ZnO nanostructures. *Appl Phys A* 124(6):458
43. Mott NF, Davis EA (2012) *Electronic processes in non-crystalline materials*. Oxford University Press
44. Oubaha M, Elmaghrum S, Copperwhite R, Corcoran B, McDonagh C, Gorin A (2012) Optical properties of high refractive index thin films processed at low-temperature. *Opt Mater* 34(8):1366–1370
45. Alsaad A, Marin CM, Alaqtash N, Chao H-W, Chang T-H, Cheung CL, Ahmad A, Qattan I, Sabirianov RF (2018) Crystallographic, vibrational modes and optical properties data of α -DIPAB crystal. *Data Brief* 16:667–684
46. Aziz SB, Abdullah OG, Brza M, Azawy AK, Tahir DA (2019) Effect of carbon nano-dots (CNDs) on structural and optical properties of PMMA polymer composite. *Results Phys* 15:102776
47. Chamroukhi H, Hamed ZB, Telfah A, Bassou M, Zeinert A, Hergenröder R, Bouchriha H (2018) Optical and structural properties enhancement of hybrid nanocomposites thin films based on polyaniline doped with Zinc Oxide embedded in bimodal mesoporous silica (ZnO@SiO_x) nanoparticles. *Opt Mater* 84:703–713
48. Sutcliffe BT, Wilson S (2003) Potential energy curves and surfaces. *Handbook of Molecular Physics and Quantum Chemistry*, pp 574–587
49. Fu DW, Zhang W, Cai HL, Ge JZ, Zhang Y, Xiong RG (2011) Diisopropylammonium chloride: a ferroelectric organic salt with a high phase transition temperature and practical utilization level of spontaneous polarization. *Adv Mater* 23(47):5658–5662
50. Jundale D, Pawar S, Chougule M, Godse P, Patil S, Raut B, Sen S, Patil V (2011) Nanocrystalline CuO thin films for H₂S monitoring: microstructural and optoelectronic characterization. *J Sens Technol* 1:36–46
51. Fasasi A, Osagie E, Pelemo D, Obiajunwa E, Ajenifuja E, Ajao J, Osinkolu G, Makinde WO, Adeoye AE (2018) Effect of precursor solvents on the optical properties of copper oxide thin films deposited using spray pyrolysis for optoelectronic applications. *Am J Mater Synth Process* 3:12–22
52. Hassanien AS, Akl AA (2015) Influence of composition on optical and dispersion parameters of thermally evaporated non-crystalline Cd₅₀S_{50-x}Se_x thin films. *J Alloys Compd* 648:280–290

Publisher's Note Springer Nature remains neutral with regard to jurisdictional claims in published maps and institutional affiliations.

Authors and Affiliations

Ahmad Telfah¹  · **Qais M. Al-Bataineh**^{1,2} · **Elen Tolstik**¹ · **Ahmad A. Ahmad**² · **Ahmad M. Alsaad**² · **Riad Ababneh**³ · **Carlos J. Tavares**⁴ · **Roland Hergenröder**¹

¹ Leibniz Institut für Analytische Wissenschaften-ISAS-e.V., Bunsen-Kirchhoff-Straße 11, 44139 Dortmund, Germany

² Department of Physical Sciences, Jordan University of Science & Technology, P.O. Box 3030, Irbid 22110, Jordan

³ Department of Physics, Yarmouk University (YU), Irbid 21163, Jordan

⁴ Centre of Physics of Minho and Porto Universities, University of Minho, 4804-533 Guimaraes, Portugal